Sensors and Actuators B 206 (2015) 364–370

Contents lists available at ScienceDirect

Sensors and Actuators B: Chemical

journal homepage: www.elsevier.com/locate/snb

Position effects of acoustic micro-resonator in quartz enhanced photoacoustic spectroscopy

Hongpeng Wu[a], Lei Dong[a,*], Wei Ren[b], Wangbao Yin[a], Weiguang Ma[a], Lei Zhang[a], Suotang Jia[a], Frank K. Tittel[b]

[a] State Key Laboratory of Quantum Optics and Quantum Optics Devices, Institute of Laser Spectroscopy, Shanxi University, Taiyuan 030006, China
[b] Department of Electrical and Computer Engineering, Rice University, Houston, TX 77004, USA

ARTICLE INFO

Article history:
Received 30 May 2014
Received in revised form 13 August 2014
Accepted 11 September 2014
Available online 20 September 2014

Keywords:
Trace gas detection
Quartz enhanced photoacoustic spectroscopy
Quartz tuning fork
Acoustic micro-resonator
Spectrophone
Position effects

ABSTRACT

The impact of acoustic micro-resonator (AmR) positions with respect to quartz tuning fork on signal amplitude, *Q*-factor and signal-to-noise ratio (SNR) of the quartz enhanced photoacoustic spectroscopy spectrophone was investigated. The replacement of the result plots' abscissas makes the highest signal amplitude and the lowest *Q*-factor for different AmRs appear at the two absolute positions, respectively. These positions are independent on the AmR geometrical parameters, which facilitates the assembly of the spectrophone. The noncoincidence between the positions of the two extreme values results in a flat peak of the SNR curve, which is different from previously reported results. The spectrophone designs for three different applications are discussed in detail.

1. Introduction

The real-time detection and quantification of trace chemical species in the gas phase has an important impact in diverse fields of applications, such as industrial process control, environmental monitoring, medical diagnostics, and automotive exhaust analysis [1–6]. Recently, there has been a growing interest in the quartz enhanced photoacoustic spectroscopy (QEPAS) technique which combines the main benefits of conventional photoacoustic spectroscopy (CPAS) with the characteristics of using a commercially available quartz tuning fork (QTF) as a resonant acoustic transducer. Due to the high quality factor Q (~12,000 in air), high resonant frequency f_0 (~32,768 Hz) and narrow resonance width (3–5 Hz) of the QTF, QEPAS is immune to ambient acoustic noise. The small size of QEPAS spectrophone as well as the cost-effectiveness is additional benefits of the QEPAS technique. In a commonly used QEPAS-based spectrophone, a so-called acoustic micro-resonator (AmR) is employed in addition to a QTF for detecting the sound signal generated by the trace gas absorbing the excitation laser beam [7–12]. With the "on-beam" configuration [7], the AmR is formed by two hypodermic, metallic thin tubes and is coupled to the QTF in order to enhance the QEPAS signal. Thus, in contrast to CPAS spectrophone including a photoacoustic cell and microphone, the optical collimating scaling requirements decrease from mms to μms, which implies that variations in the AmR position at the μm level can affect the QEPAS signal.

The performance of QEPAS spectrophone is determined by both the measurement environment and its design. The environmental parameters include electromagnetic field intensity, pressure and temperature, while the structural design includes the AmR geometrical parameters, such as shape, length, inner and outer diameters (ID and OD) and the AmR position. The influence of the electromagnetic fields on the QEPAS signal can be eliminated when an optical readout method is used, since in this case the sensor head contains no electrical components [13,14]. The pressure and temperature dependence of QEPAS spectrophone were investigated by Dong et al. [15] and Kohring et al. [16], respectively. Moreover, Dong et al. [15] studied the influence of the AmR diameter and length on the spectrophone properties. Serebryakova et al. [17] and Cao et al. [18] demonstrated that changes of the AmR length have a significant influence on QEPAS spectrophone performance. Yi et al. [19] proposed a novel T-shaped AmR to decrease the effect of viscous drag. However, the influence of the AmR position with respect to a QTF on the performance of QEPAS spectrophone has not been reported

* Corresponding author. Tel.: +86 3517018904; fax: +86 3517018927.
E-mail address: donglei@sxu.edu.cn (L. Dong).

http://dx.doi.org/10.1016/j.snb.2014.09.044
0925-4005/

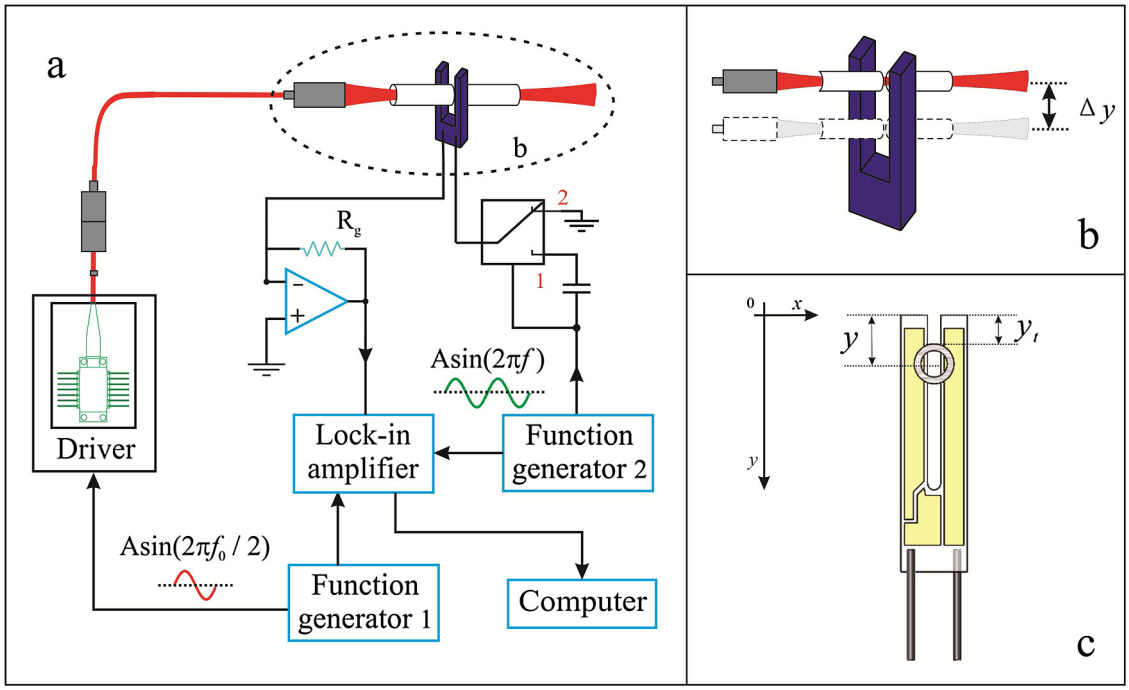

Fig. 1. (a) Schematic of the QEPAS-based experimental setup for water vapor detection. (b) Enlarged image for the QEPAS spectrophone. (c) The dimensions and coordinate system of the QTF with an AmR. The tubes were centered between the tines. y and y_t are the distances from the QTF opening to the center and the top of the tubes, respectively.

to date. Most of the previous studies mentioned above were carried out in the case that the laser beam and AmR were below the QTF opening 0.7 mm and centered between the tines which corresponds to the most sensitive position for a bare QTF. This has been confirmed theoretically and experimentally by N. Petra et al. [20] and P. Patimisco et al. [21]. However, the presence of the AmR and the interaction between the AmR and QTF alter the QTF characteristics, so that the position mentioned above is no longer optimal. The new optimal position must be experimentally determined.

In this paper, we present an experimental investigation of the AmR position effects via detecting water vapor in ambient air, with the "on-beam" configuration, at normal atmosphere pressure and temperature at ~21 °C. The QEPAS spectrophone designs for three different applications are also reported in detail.

2. Experimental optimization and results of the AmR position

A schematic of the QEPAS experimental setup for water vapor detection is shown in Fig. 1a. The experiments were carried out in two operational modes—measurement mode and calibration mode. In measurement mode, the switch in Fig. 1a was set to position 2. The detection was based on a 2f wavelength-modulation spectroscopy approach [22] by dithering and scanning the laser current. A near-infrared distributed feedback (DFB) diode laser (HuaYing Inc. Model DFB-136813C1424) with a center wavelength of 1368.7 nm and an output power of ~12.6 mW was served as the QEPAS based sensor excitation source. The DFB laser was mounted onto a custom driver board for laser temperature and current control. A sine wave supplied by a function generator 1 (Agilent Model 33210A) was applied to the driver board to modulate the laser wavelength. The modulation frequency was set to one half of the QTF resonant frequency ($f_0/2$). The function generator 2 was disabled. The output laser beam was directed into a 100 μm-diameter light spot by a fiber-coupled focuser (OZ optics model LPF-01), and then passed through the AmR and between the QTF prongs without touching any surfaces. The gaps between the QTF and the tubes were 40 μm which facilitated changing the AmR position. The tubes were centered between the QTF tines as reported in previous QEPAS publications. An H_2O line at 7299.43 cm^{-1} with an intensity of 1.008×10^{-20} $cm^{-1}/(mol\ cm^{-2})$ was chosen as the target line for demonstration. The signal produced by piezoelectric effect due to the prongs anti-symmetric vibration, were demodulated at f_0 by a lock-in amplifier (Stanford model SR830).

Two different AmRs were selected as research targets. The first AmR consists of two 4.4 mm long tubes with a 0.6 mm ID and a 0.9 mm OD, marked as AmR #1, while the second AmR is composed of two 4 mm long tubes with a 0.8 mm ID and a 1.24 mm OD, marked as AmR #2. The objective of using the two sets of AmR parameters is to further improve the previous optimized results in Refs. [15,23], which shows that the AmR #1 is the optimal AmR for a near-infrared excitation laser source, whereas the AmR #2 is more suitable AmR for the mid-infrared spectral region. The AmR and the focuser were fixed on the same holder in our experimental setup. This design ensures that the position of the laser beam with respect to AmR remains the same while the AmR is moved down along the direction of the QTF prongs, as shown in Fig. 1b. The commercially available QTF has a fork structure of two tines with a resonance frequency of 32.7 kHz. The width, length and thickness of the tine are 0.6 mm, 3.8 mm and 0.3 mm, respectively. The gap between two tines is 0.3 mm. The vertical distance between the QTF opening and the tube center was defined as y and the QTF opening is defined as zero point of y as shown in Fig. 1c.

The result of H_2O QEPAS signal amplitude for AmR #1 as a function of y is plotted in Fig. 2. The data was normalized to water concentrations to eliminate the influence caused by water vapor concentration variations. The measurement originated at the position where the tangent plane of the AmR #1 bottom just touched the top surface of the QTF tines. Therefore, the initial position of the y starts from −0.45 mm, as shown in Fig. 2. At the beginning, most of the tubes were outside the QTF tines. As the tubes moved down and overlapped with the QTF section, the coupling via the sound wave between the AmR and the QTF was established. As a result, the signal amplitude of the QEPAS spectrophone rapidly

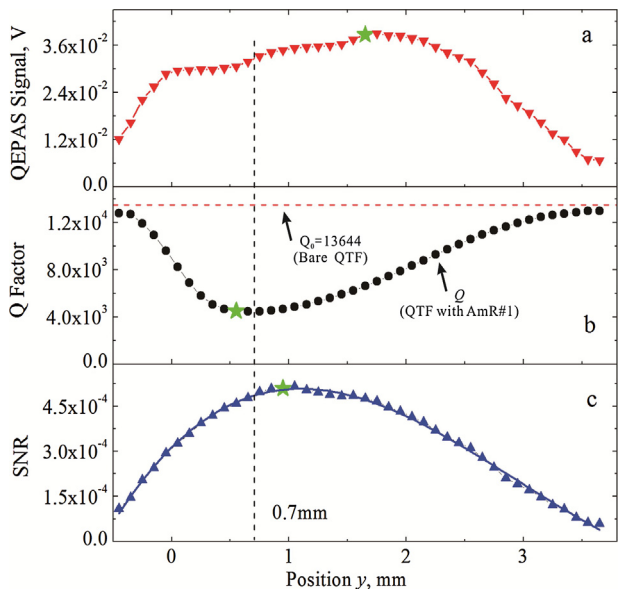

Fig. 2. The signal amplitude, Q-factor and signal-to-noise ratio as a function of the y position for AmR #1. The vertical dashed line indicates the optimum position of a bare QTF and the horizontal dashed line displays the typical Q-factor of a bare QTF. The stars mark the maximum or minimum values of the corresponding measurements.

rises with y increases in the range from −0.45 mm to 0 mm. In this case, the interaction area between the QTF and the AmR determines the signal amplitudes. After the tubes center moves below the QTF opening ($y > 0$), the signal amplitude gradually increases with y to its maximum $y = 1.75$ mm where it is close to one half of the QTF tine length. With a further increase of y, the signal amplitude decreases since it is more difficult for the AmR to vibrate the QTF prongs via pushing the lower part of two cantilever-beam-like QTF tines than the upper part.

The Q-factor is defined as the ratio of the energy stored in an oscillator to the energy supplied by a generator, per cycle. The Q-factor was measured in the calibration mode by applying an electrical sine wave excitation voltage from function generator 2 (Agilent Model 33210A) to the QTF electrode. The switch in Fig. 1a was set to position 1. The function generator 1 is disabled. The lock-in amplifier was set to 1f mode and demodulated signal. When the frequency of the excitation signal is scanned, the piezoelectric signals produced by the excited vibration were detected from the other QTF electrode. A complete QTF response profile as a function of excitation frequency was obtained, as shown in Fig. 3. The

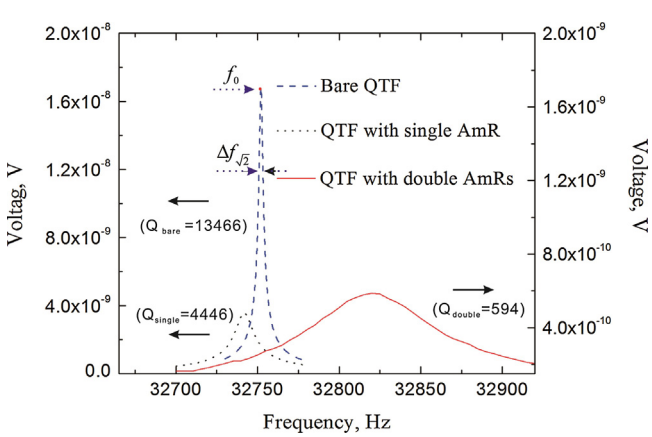

Fig. 3. A qualitative representation of the spectrophone response curves for different QEPAS based sensor configurations.

Q-factor can then be derived from the ratio of the frequency f_0 at the maximum response to the half bandwidth of the square of the response profile $\Delta f_{\sqrt{2}}$ [24]. The Q-factor can provide a measure of acoustic coupling between the QTF and the AmR. The solid line in Fig. 2b presents the variations of the measured Q-factor with the different AmR#1 positions. For comparison purpose, the typical Q-factor of a bare QTF was also plotted in Fig. 2b as horizontal dashed line. When the transfer of vibrational energy from the QTF excited by the external electrical signal to a high-loss AmR becomes more efficient, a decrease of the Q-factor is observed. The Q-factor decreases in the range of y from −0.45 mm to 0.4 mm and then remains almost constant between 0.4 mm and 0.85 mm. Subsequently, the Q-factor increases until the tubes move out of the gap between QTF prongs. The minimum Q-factor was obtained at 0.65 mm below the QTF opening (star symbol in Fig. 2b), which means that the acoustic coupling between the QTF and AmR #1 is the most efficient at this position and the high-Q QTF loses energy primarily via coupling to the low-Q AmR oscillator. However, the signal amplitude is not a maximum at the position of the lowest Q-factor comparing Fig. 2a and b. There is a 1.1 mm space between the positions of the two extreme values. A possible explanation is that the vibrational energy of the QTF is not completely transferred into sound energy of the AmR due to the presence of other types of energy dissipation. When the Q-factor is lowest, the QTF loses the most energy, but the AmR does not obtain a maximum sound energy fast enough, and vice versa.

Both signal and noise should be considered for the correct assessment of the position effects. When a QTF is represented by an equivalent serial resonant circuit, the primary QEPAS spectrophone noise is determined by the thermal noise of the QTF which can be expressed as in Refs. [25,26]:

$$\sqrt{V_{\mathrm{rms}}^2} = R_g \sqrt{\frac{4k_B T}{R}} \sqrt{\Delta f} \tag{1}$$

where $\sqrt{V_{\mathrm{rms}}^2}$ is the noise rms voltage, R_g is the value of the feedback resistor in the transimpedance amplifier, k_B is the Boltzmann constant, T is the QTF temperature, Δf is the detection bandwidth and R represents the electrical parameters of a QTF. The R value is related to other QTF parameters:

$$R = \frac{1}{Q}\sqrt{\frac{L}{C}} \tag{2}$$

where L represents the equivalent inductance and C is the equivalent capacitance. Both L and C do not change more than 0.1% with variation of y. Therefore, the noise is proportional to $\sqrt{Q}$ and thus the signal-to-noise ratio (SNR) can be estimated as the ratio of the signal amplitude to $\sqrt{Q}$ for an equivalent serial resonant circuit approximation [26]. Fig. 2c displays the calculated SNR when AmR #1 was coupled to the QTF at different positions. Unlike the signal amplitudes and Q-factor, the SNR curve is quasi-symmetric and has a top flat area. The noncoincidence between two positions of the lowest Q-factor and the highest signal amplitude results in the observed behavior of the SNR curve. The early appearance of the lowest Q-factor compensates for the lower signal amplitudes, forming a flat SNR peak.

The experimental results of the position effects of the AmR #2 are shown in Fig. 4. The curves of the signal amplitude, the Q-factor and the SNR have the same variation trend, but with a different position of the extreme values. The signal amplitudes quickly increase from −0.62 mm to 0 mm, and then rise smoothly from 0 mm to 1.98 mm. Subsequently, the signal amplitude begins to drop until the tubes are outside the gap between QTF prongs. The maximum signal amplitude appears at $y = 1.98$ mm. The position for the lowest Q-factor is $y = 0.88$ mm. The distance between the

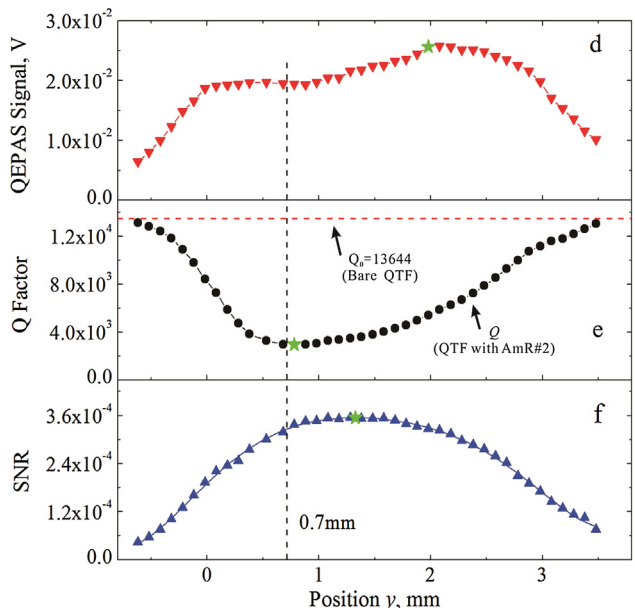

Fig. 4. The signal amplitude, Q-factor and signal-to-noise ratio as a function of the y position for AmR #2. The vertical dashed line indicates the optimum position of a bare QTF and the horizontal dashed line displays the typical Q-factor of a bare QTF. The stars indicate the maximum or minimum values of the corresponding measurements.

positions of two extreme values is 1.1 mm, which is the same as that of AMR #1. However the flat peak of SNR curve is shifted toward the right side.

The two vertical dashed lines indicate positions of $y = 0.7$ mm in Figs. 2 and 4, which were previously used as the optimal AmR mounting position. These two positions possess a lower Q-factor and are located at the edge of the flat SNR peak. Hence, their sensitivities are comparable with the optimal SNR. However, they are not positions that obtain maximum signal amplitudes. With a bare QTF, a simplified model which considers the total momentum of a gas pressure force acting on the two prongs of the QTF can predict the optimum y position [20,21]. The addition of the AmR establishes a new coupled system comprising the QTF and AmR, so that a model just considering a bare QTF is invalid. In order to predict the optimum y position, a new model consisting of the QTF and AmR must be developed.

3. Coordinate transformation

In Section 2, the vertical distance y between the QTF opening and the tube center was used as the abscissa. However, the assembly of a QEPAS spectrophone, is significant practical challenge to locate a tube center. In order to position the AmR, a practical approach is to measure the distance between the QTF opening and the tangent plane of the tube tops. Thus, a new variable y_t is defined, instead of y, as shown in Fig. 1c. The results in Figs. 2 and 4 are rearranged in Fig. 5 using the new abscissa y_t. An interesting result was observed. For the signal amplitude curves, the optimum position of the AmRs is $y_t = 1.3$ mm, regardless of the geometrical parameters of the used tubes. The lowest Q-factor occurs at $y_t = 0.2$ mm for both AmR #1 and #2. Both SNR curves have a flat peak with the same y_t range. To verify this behavior, two additional AmRs were investigated. One AmR consisted of two 4.8 mm long thin tubes with a 0.6 mm ID and a 0.9 mm OD, indicated as AmR #3. The other AmR consist of two 4.4 mm long thin tubes with a 0.8 mm ID and a 1.24 mm OD, indicated as AmR #4. The results are also shown in Fig. 5 and confirm the validity of the conclusion reported above. Therefore, using y_t as the abscissa, the extreme values of signal amplitude and Q-factor, and the range for the flat peak of the SNR appear at the same positions, respectively. As a result, it becomes practical to assemble or design a spectrophone despite of the specific AmR geometrical parameters.

4. Different QEPAS spectrophone designs

The AmR position with respect to the QTF has an effect on the signal amplitude, the spectrophone Q and SNR. This parameter has to be taken into account when designing a QEPAS spectrophone. A spectrophone with a high SNR and signal amplitude is an optimum design choice which can be realized based on the results reported in Section 3. The SNR curve for all AmRs has a flat area. The two dashed lines in Fig. 5c indicate a range from 0.06 mm to 1.36 mm for which the SNR change of AmR #2 is less than 5% compared with its highest achieved SNR. For this range, the SNR curves of the other AmRs are also flattened. Therefore, to position AmR #1 or #2 at $y_t = 1.3$ mm ($y = 1.75$ mm for AmR #1 and $y = 1.9$ mm for AmR #2), the highest signal amplitude can be achieved and the SNR remains in the flat area. Compared with the optimal position of $y = 0.7$ mm for a bare QTF, the signal amplitude for AmR #1 and #2 are enhanced ~23% and ~31%, respectively. However, the SNRs are comparable since $y_t = 1.3$ mm is located at the right hand edge of the indicated flat area, while $y = 0.7$ mm ($y_t = 0.25$ mm for AmR #1 and $y_t = 0.08$ mm for AmR #2) is located at the left hand edge of the indicated flat area.

QEPAS spectrophones have an inherently high Q-factor, resulting in long accumulation times of the acoustic energy. However, in some applications, a fast response time is required. For example, a QEPAS based sensor for clinical human breath analysis requires a response time of <1 s and a gas flow rate of <500 sccm to measure the trace gas concentration change in exhaled human breath since a typical breath cycle lasts for 15–30 s and a large gas flow rate introduces excess noise [12,27]. Thus, a high SNR spectrophone with fast dynamic characteristics is desired. The response time τ is defined as the time needed for the vibration amplitude to decay to $1/e$ of the initial value [28]. As is well known from classical oscillator theory, τ can be expressed as:

$$\tau = \frac{Q}{\pi f_0} \tag{3}$$

where f_0 is the natural vibration frequency of the oscillator. From our experimental AmR position effect investigations, the variations of f_0 were <0.03%. However, the Q-factor variations were >4 times. Consequently, the response time of a QEPAS spectrophone is mainly determined by the Q-factor. As shown in Fig. 5b, the AmR should be positioned at $y_t = 0.2$ mm ($y = 0.65$ mm for AmR #1 and $y = 0.88$ mm for AmR #2) to obtain a lower Q-factor. The two positions of y are close, but not coincident, to the optimal position of $y = 0.7$ mm for a bare QTF. Use of this position, which is still within the indicated flat SNR area, results in a ~25 ms and ~43 ms fast response time for AmR #1 and AmR #2, respectively.

The flat area of SNR curve is so sufficiently wide that it results in another benefit that allows a two detection channel design by mounting two AmRs to one QTF, as shown in Fig. 6. We refer to this innovative approach as double AmR QEPAS [29]. In this case, there is a strong coupling between two AmRs and the QTF, so that the performance characteristics of the spectrophone undergo a significant change. For example, two AmR #1s were employed to realize double AmR based spectrophone. The top AmR was positioned at $y_t = 0.2$ mm, the bottom AmR was placed at $y_t = 1.1$ mm in contact with the top AmR. In this case the QTF resonant frequency rises from 32,742 Hz to 32,841 Hz, which implies that an additional force constant is added due to the acoustic coupling. Moreover, the Q-factor decreases from ~12,000 of a bare QTF to ~600 of a double AmR based spectrophone, resulting in an ultrafast dynamic

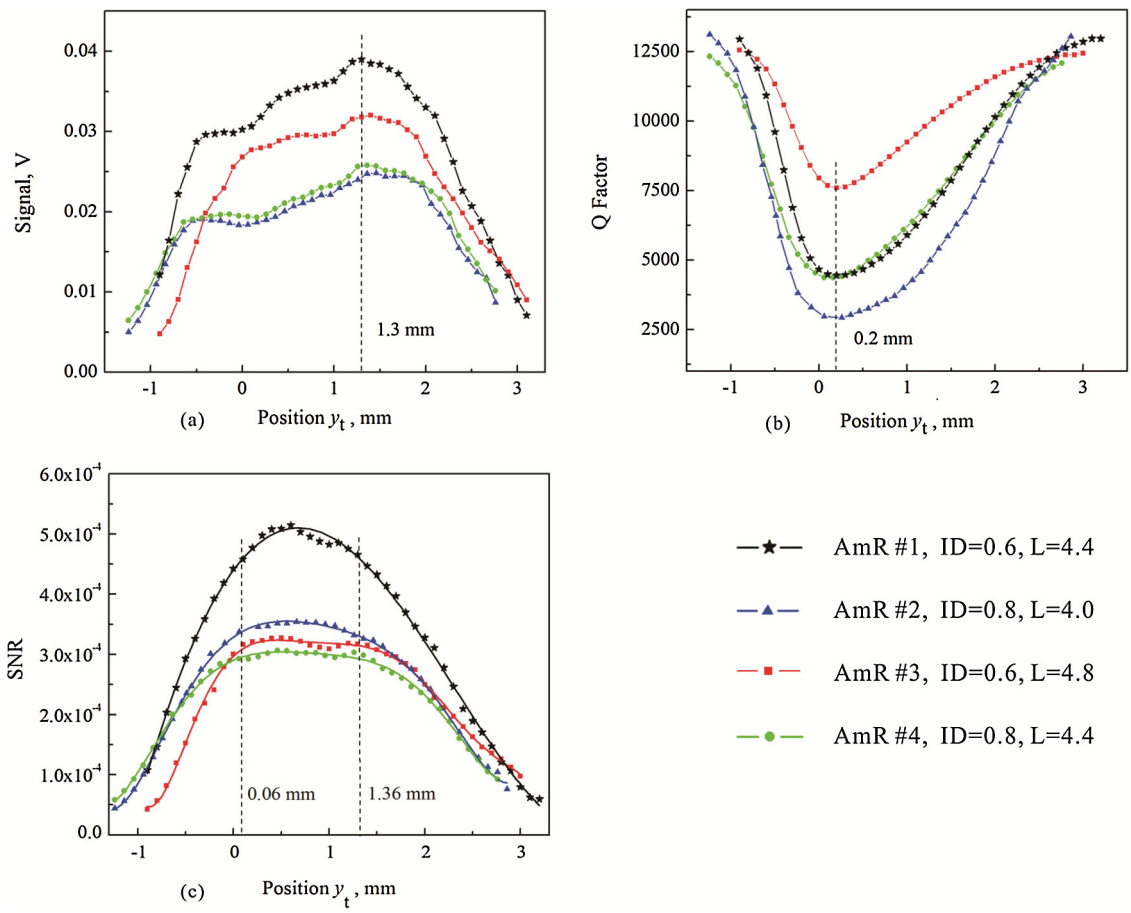

Fig. 5. Spectrophone signal amplitude, *Q*-factor and SNR as a function of the position y_t for different AmRs.

response time of ~5 ms. With such a spectrophone, the QTF response time can be improved 24 times compared with a bare QTF. Fig. 3 shows the response curves of a bare QTF, single and double AmR spectrophone. The lower *Q*-factor leads to a wider response bandwidth. Hence, the signal amplitude and phase of the double AmR spectrophone become insensitive to small drifts of the resonant frequency, compared to the high-*Q* bare QTF and single AmR spectrophone. This can extend the calibration time interval of the QEPAS sensor system. However, the double AmRs coupled to the QTF adds a dissipation channel of the vibrational energy of QTF so that a part of signal amplitude is lost. Thus, the double AmR spectrophone sensitivity is usually 5 times less than that of the single AmR spectrophone. Such a double AmR configuration can provide two advantages: (1) two laser excitation sources from

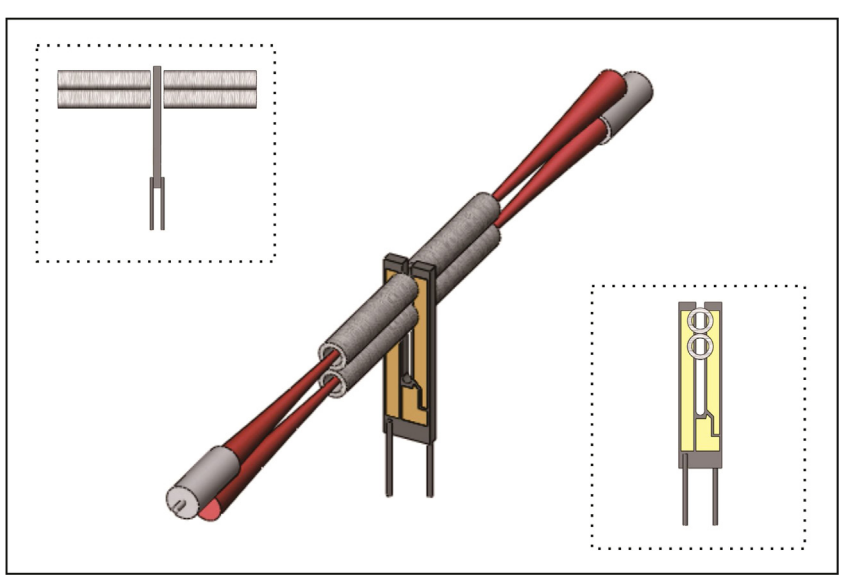

Fig. 6. Schematic of the double AmRs QEPAS.

different optical wavelengths can perform the optical signal addition or cancellation by means of the spectophone, avoiding laser beam combination and (2) the spectrophone can implement ultrafast two-gas measurements by switching two detection channels.

5. Conclusions

In summary, we have studied the position effects of the AmR in QEPAS based sensor configurations. The results show that the variations in AmR position with respect to the QTF as small as 0.1 mm can significantly affect the spectrophone performance. Therefore, accurate positioning of the AmR in spectrophone assembly is required. Using a simple replacement of the abscissas, the optimized AmR position for a high SNR and the highest signal amplitude is fixed at $y_t = 1.3$ mm, while the optimized AmR position for a high SNR and fast response time is fixed at $y_t = 0.2$ mm, regardless of the specific AmR geometrical parameters. Use of such two absolute y_t positions can facilitate positioning the AmR during the QEPAS spectrophone assembly. Furthermore, the non-coincidence between two absolute positions offers the option to realize the highest signal amplitude or a fast response spectrophone, depending on the different applications. The flat peak of the SNR curve, caused by the earlier appearance of the lowest Q-factor than the highest signal amplitude, provides the feasibility to equip the QTF with two AmRs in contact with each other, resulting in a two channels spectrophone. The reported results are extremely useful in the assembly and design of the QEPAS spectrophones.

Acknowledgements

The work was supported by the 973 program (Grant No. 2012CB921603), National Natural Science Foundation of China (Grant Nos. 61275213, 61108030, 61127017, 61178009, 61378047, and 61205216), the National Key Technology R&D Program (2013BAC14B01), the Shanxi Natural Science Foundation (Grants 2013021004-1, and 2012021022-1), the Shanxi Patent Promotion and Implementation Project, and the Shanxi Scholarship Council of China (2013-011, 2013-01) and the Robert Welch Foundation grant C-0586.

References

[1] A.A. Kosterev, G. Wysocki, Y. Bakhirkin, S. So, R. Lewicki, M. Fraser, F.K. Tittel, R.F. Curl, Application of quantum cascade lasers to trace gas analysis, Appl. Phys. B 90 (2008) 165–176.
[2] L. Dong, W. Yin, W. Ma, L. Zhang, S. Jia, High-sensitivity, large dynamic range, auto-calibration methane optical sensor using a short confocal Fabry–Perot cavity, Sens. Actuators B 127 (2007) 350–357.
[3] S. Borri, P. Patimisco, A. Sampaolo, H.E. Beere, D.A. Ritchie, M.S. Vitiello, G. Scamarcio, V. Spagnolo, Terahertz quartz enhanced photo-acoustic sensor, Appl. Phys. Lett. 103 (2) (2013) 021105.
[4] Z. Li, L. Zhao, W. Tan, W. Ma, G. Zhao, X. Fu, L. Dong, L. Zhang, W. Yin, S. Jia, Investigation and cancellation of residual amplitude modulation in fiber electro-optic modulator based frequency modulation gas sensing technique, Sens. Actuators B 196 (2014) 23–30.
[5] P. Ehlers, I. Silander, J. Wang, A. Foltynowicz, O. Axner, Fiber-laser-based noise-immune cavity-enhanced optical heterodyne molecular spectrometry incorporating an optical circulator, Opt. Lett. 39 (2) (2014) 279–282.
[6] Y. Cao, W. Jin, L. Ho, Z. Liu, Evanescent-wave photoacoustic spectroscopy with optical micro/nano fibers, Opt. Lett. 37 (2) (2012) 214–216.
[7] A.A. Kosterev, Y.A. Bakhirkin, R.F. Curl, F.K. Tittel, Quartz-enhanced photoacoustic spectroscopy, Opt. Lett. 27 (21) (2002) 1902–1904.
[8] V. Spagnolo, P. Patimisco, S. Borri, G. Scamarcio, B.E. Bernacki, J. Kriesel, Part-per-trillion level detection of SF_6 using a single-mode fiber-coupled quantum cascade laser and a quartz enhanced photoacoustic sensor, Opt. Lett. 37 (21) (2012) 4461–4463.
[9] Y. Ma, R. Lewicki, M. Razeghi, F.K. Tittel, QEPAS based ppb-level detection of CO and N_2O using a high power CW DFB-QCL, Opt. Express 21 (1) (2013) 1008–1019.
[10] S. Borri, P. Patimisco, I. Galli, D. Mazzotti, G. Giusfredi, N. Akikusa, M. Yamanishi, G. Scamarcio, P.D. Natale, V. Spagnolo, Intracavity quartz-enhanced photoacoustic sensor, Appl. Phys. Lett. 104 (9) (2014) 091114.
[11] H. Yi, K. Liu, W. Chen, T. Tan, L. Wang, X. Gao, Application of a broadband blue laser diode to trace NO_2 detection using off-beam quartz-enhanced photoacoustic spectroscopy, Opt. Lett. 36 (4) (2011) 481–483.
[12] L. Dong, J. Wright, B. Peters, B.A. Ferguson, F.K. Tittel, S. McWhorter, Compact QEPAS sensor for trace methane and ammonia detection in impure hydrogen, Appl. Phys. B 107 (2012) 459–467.
[13] M. Köhring, A. Pohlkötter, U. Willer, M. Angelmahr, W. Schade, Tuning fork enhanced interferometric photoacoustic spectroscopy: a new method for trace gas analysis, Appl. Phys. B 102 (2011) 133–139.
[14] Y. Liu, L. Dong, H. Wu, H. Zheng, W. Ma, L. Zhang, W. Ying, Q. Zhu, W. Yin, S. Jia, All optical quartz-enhanced photoacoustic spectroscopy, Acta Phys. Sin. 62 (7) (2013) 220701.
[15] L. Dong, A.A. Kosterev, D. Thonazy, F.K. Tittel, QEPAS spectrophones: design, optimization, and performance, Appl. Phys. B 100 (2010) 627–635.
[16] M. Köhring, S. Böttger, U. Willer, W. Schade, Temperature effects in tuning fork enhanced interferometric photoacoustic spectroscopy, Opt. Express 21 (18) (2013) 20911–20922.
[17] D.V. Serebryakova, I.V. Morozova, A.A. Kosterevb, V.S. Letokhova, Laser microphotoacoustic sensor of ammonia traces in the atmosphere, Quant. Electron. 40 (2) (2010) 167–172.
[18] Y. Cao, W. Jin, L. Ho, Optimization of spectrophone performance for quartz-enhanced photoacoustic spectroscopy, Sens. Actuators B 174 (2012) 24–30.
[19] H. Yi, W. Chen, S. Sun, K. Liu, T. Tan, X. Gao, T-shape microresonator-based high sensitivity quartz-enhanced photoacoustic spectroscopy sensor, Opt. Express 20 (8) (2012) 9187–9196.
[20] N. Petra, J. Zweck, A.A. Kosterev, S.E. Minkoff, D. Thomazy, Theoretical analysis of a quartz-enhanced photoacoustic spectroscopy sensor, Appl. Phys. B 94 (2009) 673–680.
[21] P. Patimisco, G. Scamarcio, F.K. Tittel, V. Spagnolo, Quartz-enhanced photoacoustic spectroscopy: a review, Sensors 14 (4) (2014) 6165–6206.
[22] D. Rojas, P. Ljung, O. Axner, An investigation of the 2f-wavelength modulation technique for detection of atoms under optically thin as well as thick conditions, Spectrochim. Acta B 52 (1997) 1663–1686.
[23] L. Dong, V. Spagnolo, R. Lewicki, F.K. Tittel, Ppb-level detection of nitric oxide using an external cavity quantum cascade laser based QEPAS sensor, Opt. Express 19 (24) (2011) 24037–24045.
[24] A.A. Kosterev, F.K. Tittel, D.V. Serebryakov, A.L. Malinovsky, I.V. Morozov, Applications of quartz tuning forks in spectroscopic gas sensing, Rev. Sci. Instrum. 76 (2005) 043105.
[25] R.D. Grober, J. Acimovic, J. Schuck, D. Hessman, P.J. Kindlemann, J. Hespanha, A.S. Morse, Fundamental limits to force detection using quartz tuning forks, Rev. Sci. Instrum. 71 (2000) 2776–2780.
[26] A.A. Kosterev, F.K. Tittel, Ammonia detection by use of quartz-enhanced photoacoustic spectroscopy with a near-IR telecommunication diode laser, Appl. Opt. 43 (33) (2004) 6213–6217.
[27] J.P. Waclawek, R. Lewicki, H. Moser, M. Brandstetter, F.K. Tittel, B. Lendl, Quartz-enhanced photoacoustic spectroscopy-based sensor system for sulfur dioxide detection using a CW DFB-QCL, Appl. Phys. B (2014), http://dx.doi.org/10.1007/s00340-014-5809-y.
[28] A.A. Kosterev, P.R. Buerki, L. Dong, M. Reed, T. Day, F.K. Tittel, QEPAS detector for rapid spectral measurements, Appl. Phys. B 100 (2010) 173–180.
[29] L. Dong, H. Wu, H. Zheng, Y. Liu, X. Liu, W. Jiang, L. Zhang, W. Ma, W. Ren, W. Yin, S. Jia, F.K. Tittel, Double acoustic micro-resonator quartz enhanced photoacoustic spectroscopy, Opt. Lett. 39 (8) (2014) 2479–2482.

Biographies

Hongpeng Wu received his B.S. degree in physics from Shanxi University, China, in 2011. He is now pursuing the Ph.D. degree of atomic and molecular physics from the Institute of Laser Spectroscopy in Shanxi University. His research interests include gas sensors, photoacoustic spectroscopy, and laser spectroscopy technique.

Lei Dong received his Ph.D. degree in optics from Shanxi University, China, in 2007. June 2008–December 2011, he worked as a post doctor in Rice University, USA. Now he is an associate professor of Shanxi University. His research interests include optical sensors, trace gas detection, and laser spectroscopy.

Wei Ren is currently a postdoctoral researcher in Electrical Computer Engineering Department at Rice University. He received his Ph.D. degree in Mechanical Engineering from Stanford University in 2013. His research interests include trace gas detection using laser spectroscopy, combustion and propulsion systems.

Wangbao Yin received his B.S. in physics from Shanxi University, China, in 1986, and the Ph.D. degree in laser spectrum laboratory from Shanxi University, China, in 2003. He is currently a professor in Institute of Laser Spectroscopy. His research interests are environmental sensors, flexible electronic packaging, and application of laser spectroscopy.

Weiguang Ma received his Ph.D. degree in optics from Shanxi University, China, in 2005. April 2006–January 2009, he worked as a post doctor in Department of Physics in Umeå University, Sweden. Now he is an associate professor of Shanxi University. His research interests include optical parameter oscillation, sum frequency generation, highly sensitive laser spectroscopy, and trace gas detection.

Lei Zhang received his Ph.D. degree in atomic and molecular physics from Shanxi University, China, in 2008. Now he is an associate professor of Shanxi University. His research interests include laser-induced breakdown spectroscopy and highly sensitive laser spectroscopy.

Suotang Jia received his B.S. degree in physics in 1986 and the M.S. degree in optics in 1989 from Shanxi University, China. He graduated with the Ph.D. degree for research on laser spectroscopy in 1994 from East China Normal University. Since 1996, he has worked as a visiting scholar in CNRS in France, University of Maryland, Yale University, University of Connecticut and so on. He now is a professor in Shanxi University and became the president of Shanxi University in 2012. His research interests include quantum optics, quantum information, ultracold atom and molecular, and application of laser spectroscopy.

Frank K. Tittel received his B.S. degree in 1955 and the Ph.D. degree in 1959 from Oxford University. Now he is J.S. Abercrombie professor in Rice University, USA. Professor Frank Tittel has been involved in many innovative developments in quantum electronics and laser technology since the discovery of the laser in 1960, with applications ranging from laser spectroscopy to environmental monitoring. The most recent designs utilize novel quantum cascade lasers to achieve compact, robust instrumentation that can be deployed for field applications, such as at NASA's Johnson Space Center related to air and water quality issues relevant to the International Space Station, by the Environmental Protection Agency for urban formaldehyde monitoring, and by the National Institute of Health for non-invasive NO and CO detection in biomedical systems.